Dual Mesomorphic Assemblage of Chitin Normal Acylates and Rapid Enthalpy Relaxation of Their Side Chains

Yoshikuni Teramoto,† Tomoya Miyata, and Yoshiyuki Nishio*

Division of Forest and Biomaterials Science, Graduate School of Agriculture, Kyoto University, Sakyo-ku, Kyoto 606-8502, Japan

Received August 15, 2005; Revised Manuscript Received November 5, 2005

Chitin derivatives having normalacyl groups ($C_nH_{2n-1}O-$; $n = 4-20$) were synthesized with pyridine, *p*-toluenesulfonyl chloride, and normal alkanoic acid in an *N*,*N*-dimethylacetamide-lithium chloride homogeneous system. The products (C_n-ACs; degree of acyl substitution, DS = 1.7−1.9) showed an *n*-dependent thermal transition behavior: no evident transition ($n = 4-10$), a glass transition ($n = 12$ and 14), and a pseudo-first-order phase transition ($n = 16-20$), the latter two occurring usually below room temperature when examined by differential scanning calorimetry. Wide-angle X-ray diffractometry (WAXD) at 20 °C displayed a sharp diffraction peak ($2\theta = 2°-7°$) and a diffuse halo ($2\theta \approx 20°$) for the respective C_n-ACs. The former *d*-spacing (1.5−3.6 nm) increased with an increase in *n* to yield two stages of mutually different increasing rates, which reflects a systematic *n*-dependence of the period of a layered structure of the main chains. The molecular assembly of C_n-ACs exhibited "dual mesomorphy"; nematic ordering for the semirigid carbohydrate trunk and smectic one for the flexible side chains. On the other hand, WAXD profiles of C_n-ACs ($n = 14-18$) indicated almost no temperature dependence from −150 to +220 °C. Therefore, it was reasonably assumed that the pseudo-first-order transition observed in thermograms of C_n-ACs ($n = 16-20$) was due to the enthalpy relaxation of the side-chain assemblage. An insight was provided into the kinetics of the characteristic aging behavior as a liquid-crystalline glass, in comparison with the corresponding data for other noncrystalline macromolecules.

1. Introduction

Chitin, which is supplied in abundance by marine crustaceans, is a representative of a naturally occurring polysaccharide derived from animal sources. It is structurally similar to cellulose and may be regarded as cellulose with the hydroxyl group at position C2 replaced by an acetylamino group. However, the difference between chitin and cellulose arises due to the presence of amino groups in the former, which is advantageous in that it provides distinctive biological functions, for example, bioassimilability and antibacteriality. Therefore, chitin is expected to have a large potential for functionalization in medical, pharmaceutical, food, and textile industries.

To apply these fascinating properties, a number of studies have been conducted on the chemical modifications of chitin molecules.[1,2] However, chitin is generally modified by reactions under heterogeneous conditions. Usually, such reactions are accompanied by various problems such as poor extent of reaction, structural nonuniformity of the products, and partial degradation of the products under severe reaction conditions. The solvent *N*,*N*-dimethylacetamide (DMAc)-lithium chloride (LiCl) is known as a "true solvent" of chitin as well as cellulose in which no appreciable degradation of the molecules occurs. This solvent has been utilized effectively to prepare chitin-based polyblends.[3−6] Numerous studies on the chemical modifications of cellulose have also been conducted;[7] however, there exist only a small number of instances of chitin derivatization via the homogeneous system in DMAc−LiCl.[8−11]

With regard to the practical applications of chitin and its derivatives, it is essential to formulate the correlation between their structure and material properties. However, only a few systematic studies dealing with morphology, thermal behavior, and mechanical properties of "chitinous polymers" are obtainable. In contrast, many extensive structural and physical studies have been conducted with regard to "cellulosics." One possible reason for this disparity is the predominance of heterogeneous modifications of chitin. It is much more desirable to perform the reactions in homogeneous solution and under mild conditions so that the respective derivatives can be analyzed as homogeneous materials. This will contribute significantly toward establishing a general scheme of the physicochemical characteristics of chitin derivatives coupled with expanding their practical usage including the utilization of the biologically specific benefits as aminopolysaccharide.

This paper is concerned with the synthesis of a series of chitin alkyl ester derivatives. Normal acyl groups ($C_nH_{2n-1}O-$; $n = 4-20$) were introduced as substituent sequences. The normal acylated chitins (C_n-ACs) were prepared with *p*-toluenesulfonyl chloride and normal alkanoic acid in the presence of a pyridine catalyst in a DMAc−LiCl homogeneous system based on previous reports on an effective acylation system for cellulose.[12] The reaction system is known to yield cellulose esters with fairly longer acyl side chains such as stearyl groups.[13] Another objective of this study is to elucidate the relationship between the molecular structure, thermal transition behavior, and supramolecular architecture. Similarly, attention has been focused on fatty acid esters of starch,[14] cellulose,[13] and chitosan[15] from the viewpoint of utilizing them as novel biodegradable thermoplastic polymers. These studies indicated that the longer side chains arranged themselves in a pseudocrystalline structure. In this study, we aim to propose an alternative model of supra-

* To whom correspondence should be addressed. E-mail: ynishio@kais.kyoto-u.ac.jp. Tel.: +81 75 753 6250. Fax: +81 75 753 6300.

† Present address: Biomass Technology Research Center (BTRC), National Institute of Advanced Industrial Science and Technology (AIST) 2-2-2, Hirosuehiro, Kure, Hiroshima 737-0197, Japan.

10.1021/bm050580y CCC: $33.50
Published on Web 12/10/2005

molecular structure for this acylated derivative series of chitin by the combined use of differential scanning calorimetory (DSC) and thermoregulated, wide-angle X-ray diffractometory (WAXD). The kinetic analysis of the thermal behavior of the longer side chains is also conducted to quantitatively support the novel structural model.

2. Experimental Section

2.1. Original Materials. The original chitin material isolated from crab shells (Fluka 22720 Chitin Lot & Filling code: 405226/1 12900) was purified by treatment with aqueous hydrochloric acid and sodium hydroxide solution according to Hackman's method.[16] The nominal molecular weight of the chitin material is 4×10^5. The degree of deacetylation (DD) of the purified chitin (p-chitin) was 9.8%, determined by infrared spectroscopy.[17] Reagent-grade *N*,*N*-dimethylacetamide (DMAc) was stored over molecular sieves 3A before use. Lithium chloride (LiCl) was dried at 120 °C for 12 h in a vacuum oven. *p*-Toluenesulfonyl chloride (TsCl) and butylic (C_4), hexanoic (C_6), octanoic (C_8), decanoic (C_{10}), lauric (C_{12}), myristic (C_{14}), palmitic (C_{16}), stearic (C_{18}), and eicosanoic (C_{20}) acids (C_n-acids) were obtained from Wako Pure Chemical Industries Ltd. or Aldrich Chemical Co. and used as received. Other reagents were purchased from Nacalai Tesque Co. or Wako Pure Chemical Industries Ltd. and used as received.

2.2. Preparation of Chitin Solution. The purified chitin sample was first treated with water, methanol, and DMAc in succession by a solvent exchange technique.[18,19] The DMAc-wet chitin was then added to a solvent system DMAc−LiCl and stirred at room temperature for about 5 days. The solvent DMAc−LiCl was used at a salt concentration of 9 wt % with respect to DMAc. The actual concentration of chitin in the clear solution was controlled at ca. 0.3 wt %; this was determined precisely by weighing the solid film regenerated from a portion of the solution.

2.3. Acylation of Chitin. A solution of pyridine (12 eq/anhydroglucosamine residue) in DMAc was added dropwise to 50 mL of a 0.3 wt % solution of chitin in DMAc−LiCl at 20 °C. Subsequently, a solution of alkanoic acid (8 eq/chitin OH) in DMAc was added to the chitin solution, followed by the addition of a solution of TsCl (8 eq/chitin OH) in DMAc. The molar ratios of the respective couples of the reagent/DMAc were fixed at 1:1. The system was then heated to 50 °C and maintained at this temperature for 100 h except in the case of acylation with eicosanoic acid (C_{20}), when the temperature was 65 °C to expedite the dissolution of the C_{20}-acid. The above procedures were conducted with vigorous stirring under a nitrogen atmosphere. The acylated products were recovered as white or light-yellow powders by precipitation in methanol (for C_4- to C_{14}-AC) or diethyl ether (for C_{16}- to C_{20}-AC), washed successively with the respective solvents for 12 h, and dried at 55 °C in vacuo for 12 h.

2.4. Measurements. The Fourier transform infrared (FT-IR) spectra of p-chitin and C_n-AC samples were obtained using a Shimadzu FTIR-8600 spectrometer. A standard KBr-pellet method was employed for all the measurements.

The 300-MHz ^{1}H NMR spectra of the C_n-AC samples were recorded using a Varian INOVA 300 FT-NMR apparatus. The measurement conditions were as follows: solvent, $CDCl_3/CF_3COOD$ (1/4 in volume); solute concentration, 15 mg mL^{-1}; internal standard, tetramethylsilane; temperature, 17 °C; number of scans, 128. The degree of normal acyl substitution (DS) of the C_n-AC samples was determined by the ^{1}H NMR spectra measurements, where the intensity of the methyl-group proton signals ($\delta = 0.8-1.1$ ppm) was compared with that of the signals ($\delta = 3.5-5.6$ ppm) from the chitin backbone protons located in the anhydroglucosamine unit. The WAXD measurements at 20 °C were carried out using a Rigaku RINT2200V. Nickel-filtered Cu Kα radiation ($\lambda = 0.1542$ nm) was used at 40 kV and 30 mA. The WAXD measurements over a temperature range of −150 to +200 °C at a heating rate of 10 K min^{-1} were carried out using a Rigaku RINT-Ultima II equipped with an attachment for medium- and low-temperature diffractometry, where the nickel-filtered Cu Kα radiation was used at 50 kV and 40 mA. The data were recorded every 10 degrees after maintaining a preestablished temperature for 5 min. The diffraction intensity profiles were uniformly collected in a range of $2\theta = 2°-45°$.

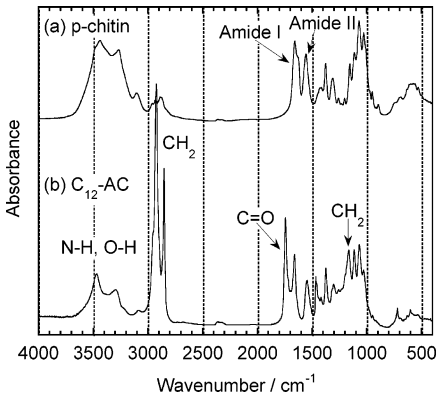

Figure 1. FT-IR spectra of (a) p-chitin and (b) C_{12}-AC.

DSC was performed using a Seiko DSC6200/EXSTAR6000 apparatus. The measurements were carried out by using 3−5 mg samples under a nitrogen atmosphere after calibrating the temperature readings with an indium standard. The samples were first heated from −140 to +200 °C at a scanning rate of 20 K min^{-1} (first heating scan) and then immediately quenched to −140 °C at a rate of about 80 K min^{-1}. The second heating scans were run from −140 to +200 °C at a scanning rate of 20 K min^{-1} to record stable thermograms. Subsequently, the cooling scans were examined from +200 to −140 °C at a scanning rate of 20 K min^{-1}.

Another series of DSC measurements was conducted in order to evaluate the enthalpy relaxation behavior of the normal acyl side chains of $n \geq 16$. The following procedure was adopted for this experiment, which is usually termed the constant cooling rate experiment. For any C_n-AC of $n = 16-20$, a single sample was used throughout. The sample was initially heated in the DSC apparatus at 20 K min^{-1} to 150 °C so as to erase its thermal history. It was then cooled at 10 K min^{-1} to −140 (C_{16}), −120 (C_{18}), and −100 °C (C_{20}) and immediately reheated at 10 K min^{-1} to 150 °C. This procedure was repeated with other cooling rates of 7.5, 5.0, 2.5, and 1.2 K min^{-1}.

3. Results and Discussion

3.1. Spectroscopic Characterization of C_n-AC Products. Figure 1 displays the FT-IR spectra of p-chitin and a selected C_n-AC ($n = 12$). As can be seen comparatively from the spectra, the major absorption in p-chitin, which is ascribed to O−H and N−H stretching bands, occurs in the range of 3000−3700 cm^{-1}. However, these bands are suppressed after the acylation. Instead, in the acylated chitin, a remarkable development in absorption was observed in the following two regions: 2800−3000 cm^{-1} (CH_2 stretching of normal acyl side chains) and 1750 cm^{-1} (ester C═O stretching). The lower frequency portion of the amide I doublet (1627 cm^{-1}) disappeared, thereby implying the suppression of the intramolecular hydrogen bondings of the C═O with O6H and/or N−H.[20,21] Thus, the FT-IR measurements indicated sufficient progress of the acylation and confirmed the degeneration of the intramolecular hydrogen bondings of the chitin starting material for all C_n-AC products of $n = 4-20$.

Figure 2 depicts a ^{1}H NMR spectrum obtained for the C_{12}-AC sample. A signal due to **a**-methylene protons (see structural formula inserted in Figure 2) of the normal alkyl ester side chains was detected at 2.55 ppm. If the acyl substitution occurred at the N2H position, the protons on the **a**-methylene carbon of the resulting amide attached to the pyranose ring would yield a

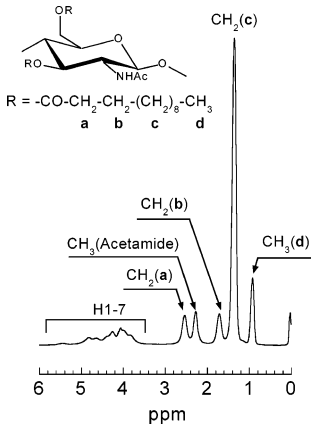

Figure 2. ^{1}H NMR spectrum of C_{12}-AC in $CDCl_3/CF_3COOD$ (1/4 in volume).

Table 1. Preparation Conditions of C_n-ACs ($n = 4-20$) and Their DS and DD Values

sample code	reaction temp./°C	alkanoic acid/ TsCl/pyridine[a]	DS	DD (%)
C_4-AC	50	8/8/12	1.80	10.5
C_6-AC	50	8/8/12	1.84	10.2
C_8-AC	50	8/8/12	1.80	13.1
C_{10}-AC	50	8/8/12	1.83	14.2
C_{12}-AC	50	8/8/12	1.80	13.7
C_{14}-AC	50	8/8/12	1.79	14.0
C_{16}-AC	50	8/8/12	1.85	15.5
C_{18}-AC	50	8/8/12	1.78	13.6
C_{20}-AC	65	8/8/12	1.65	13.2

[a] Represented by the molar ratio to one repeating unit of chitin.

peak maximum between the signal of the **a**-proton via ester linkage and that of the methyl protons of the innate acetamide.[22] However, careful observation revealed that no peak or shoulder appeared in the range 2.3−2.5 ppm. Thus, the present acylation was found to occur mainly at the O3H and/or O6H positions of the pyranose ring, yielding the chitin ester derivatives with DS $\leq$ 2 and preserving the original acetamide group in general.

In the spectrum shown in Figure 2, we designate a resonance peak area derived from the terminal methyl (**d**) protons of normal acyl groups as **A**; an area from the methyl protons of acetamide, **B**; and a broad and overlapping area from the 7 protons of anhydroglucose residue, **C**. The values of the degree of deacetylation (DD, in percent) and DS can be estimated by eqs 1 and 2, respectively

$$\mathrm{DD} = 100(1 - 7\mathbf{B}/3\mathbf{C}) \quad (1)$$

$$\mathrm{DS} = 7\mathbf{A}/3\mathbf{C} \quad (2)$$

The result of the characterization is summarized in Table 1. It is evident from the data that the DD values around 13% are comparable to that (9.8%) determined by FT-IR for the starting p-chitin. Therefore, lesser deacetylation of the chitin backbone occurred during the course of the acylation under the currently adopted condition. The DS values of C_n-ACs were determined to be around 1.8, which are comparable to a maximum possible DS of two hydroxyls for substitution per chitin repeat unit. Considering the predominance of the esterification revealed by the FT-IR and ^{1}H NMR analyses, it can be concluded that almost saturated esters of chitin were obtained by this acylation reaction.

3.2. Structure of C_n-ACs at Ambient Temperature. Figure 3 illustrates the WAXD intensity profiles obtained at 20 °C for powder samples of the original p-chitin and as-prepared C_n-

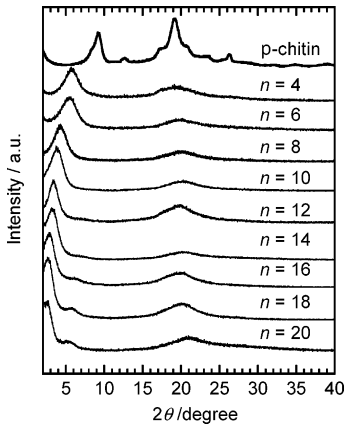

Figure 3. WAXD profiles of p-chitin and C_n-ACs ($n = 4-20$) measured at 20 °C.

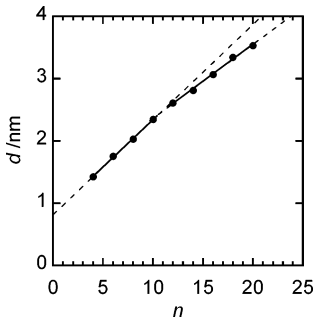

Figure 4. Plots of the *d*-spacing of C_n-ACs ($n = 4-20$) calculated from the peak position at lower diffraction angles ($2\theta = 2°-7°$) as a function of the number of carbon atoms in the side chains.

ACs. All of the C_n-ACs yield a fairly sharp diffraction peak with a maximum at $2\theta = 2°-7°$, and a broad halo centering 18°−21° which is characteristic of noncrystalline materials exhibiting only an ill-defined short-range order. With an increase in the number *n* of carbon atoms in the normal acyl substituents of C_n-ACs, the former peak gradually shifted to smaller diffraction angles. Therefore, based on this result, it may be considered that the main chains were arranged in a regular, layered array with their side chains between the layers, but without any definite longitudinal periodicity. A similar diffraction behavior in such lower-angle regions has been observed for other polymers with flexible side chains.[23−29] Very small diffraction peaks detected at $2\theta = 5°-8°$ for the C_n-ACs with longer side chains ($n \geq 12$) should be attributed to a secondary diffraction of the periodic layered structure of the main chain, which becomes more prominent with increasing *n*. On the other hand, as deduced from the absence of the detection of any acute diffraction other than that at $2\theta = 2°-7°$ in the present WAXD measurements, the acyl side chains never generate any crystalline lattice structure among themselves at a room temperature of 20 °C (refer to Figure 7).

To estimate the characteristic repeating distance from the respective low-angle peak positions, we applied the Bragg's law, $\lambda = 2d \sin \theta$. The corresponding *d* values are plotted as a function of *n* in Figure 4. Based on the observation of the regular increment in the *d*-spacing with increasing *n*, a fairly oriented structure of the normal acyl side chains is allowable despite the absence of structural regularity in the crystallographic sense described above. However, the *d*-spacing versus *n* plot yields an inflection point at $n = 10$ or 12, suggesting that, at the critical carbon number, a change takes place concerning the manner of the side-chain packing between trunk polymer chains. Below

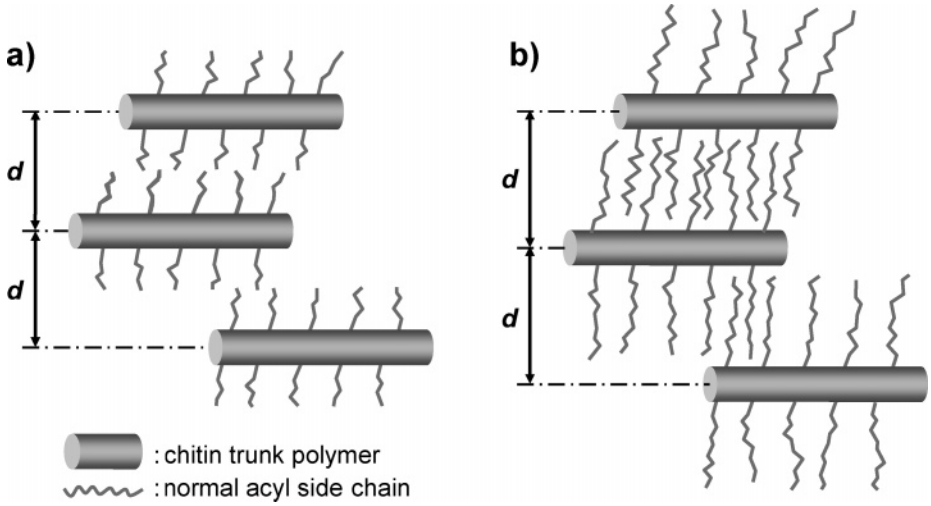

Figure 5. Schematic representations of the layered structure of C_n-ACs with their side chains arranged in an (a) end-to-end nonoverlapping or (b) interdigitating fashion.

the critical side-chain length ($n \leq 10$), there is a linear increase in the periodicity at a rate of 0.152 nm/CH_2. When the side-chain length is in the range $n = 12-20$, another linear increase in the packing periodicity is observed, and the rate diminishes to 0.119 nm/CH_2.

We estimated the diameter of the chitinous trunk chain to be 0.94 nm,[30] which corresponds to half the lattice constant of a longer axis perpendicular to the molecular axis. Considering the diameter together with the double lengths of ester linkage (0.27 nm), the total projecting length (1.21 nm) is greater than an extrapolated *d*-spacing of the larger slope at $n = 1$ (0.97 nm) in the plot shown in Figure 4. Moreover, the value of the intercept in the plot for $n = 0$, 0.82 nm, is smaller than that for the trunk diameter, 0.94 nm. It is therefore suggested that the side chains or parts of individual side chains are not perpendicular to the molecular axis but slightly tilted at a small angle to the normal axis.

Potential models of the side-chain packing in the layered structure of C_n-ACs are illustrated in Figure 5. Model b of interdigitation should provide a rate less than 0.125 nm/CH_2 with regard to the *d*-spacing elevation with *n* because of the tilting of the side chain; the value 0.125 nm corresponds to the unit height per carbon of an alkyl chain. On the other hand, model a indicates a nonoverlapping end-to-end packing arrangement, which implies that the increasing rate of the *d*-spacing with *n* should be less than 0.25 nm/CH_2. In the case of the acylated products of $n \leq 10$, where the observed increment in the *d*-spacing for each CH_2 was 0.152 nm, it may be presumed that the side chains are prone to assume a less-overlapping end-to-end packing fashion comparable to model a. On the other hand, the observation for the side chains of $n = 12-20$, that is, the smaller increment in the *d*-spacing (0.119 nm) per CH_2, indicates the prevalence of the interdigitated packing (Figure 5b). A possible explanation for this origin is that the terminal portion of the longer side chains has a higher mobility with lesser influence of one-end-anchoring[31] onto the semirigid chitin backbone. The lower conformational restraint for the longer side chains would result in a relatively free association, thereby allowing their interdigitation as well as their partial mutual intertwining. However, at least at an ambient temperature, even the interdigitated side-chain assembly failed to form any ordered crystalline lattice, as has been evidenced by the fact that no sharp diffraction peak was observed at higher angular positions in the WAXD profiles (at 20 °C).

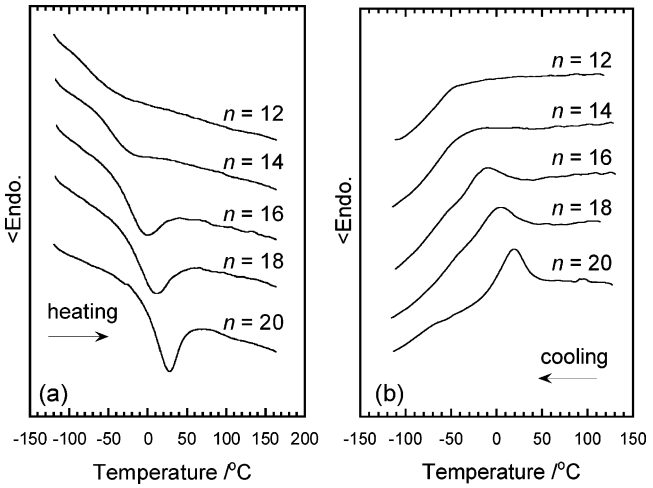

Figure 6. DSC thermograms of C_n-ACs obtained in (a) the second heating scan and (b) the following cooling scan, each recorded at a scanning rate of 20 K min^{-1}.

3.3. Thermal Transition Behavior of C_n-ACs. The C_n-AC samples were examined in the thermal analysis by DSC to clarify the *n*-dependence of the transition behavior. Figure 6a displays the thermograms of selected C_n-ACs ($n = 12-20$) in the second heating scan conducted at a scanning rate of 20 K min^{-1} after rapid quenching from 200 °C. Figure 6b depicts the DSC thermograms of the same C_n-AC samples in the cooling scan following the second heating. The respective cooling data impart a transition signal that is inverted with respect to that observed in a somewhat higher temperature region in the preceding heating scans. A series of DSC measurements revealed that the thermal transition behavior of C_n-ACs can be grouped into three classes based on the value of *n*: no evident transition for $n = 4-10$; glass transition with the midpoint in a range of −70 to −40 °C for $n = 12$ and 14; pseudo-first-order phase transition with an endothermic maximum in a range of −10 to +30 °C for $n = 16-20$.

The temperature (20 °C) for the preceding WAXD measurements is higher than the transition temperature limits for $n = 12$ and 14 and comparable with those for $n = 16-20$. In view of the result that the WAXD data clearly indicated a sharp diffraction peak at $2\theta = 2°-7°$ due to the layered structure of the main chain, the thermal behavior observed above is not likely to be derived from transitions associated with the chitin trunk

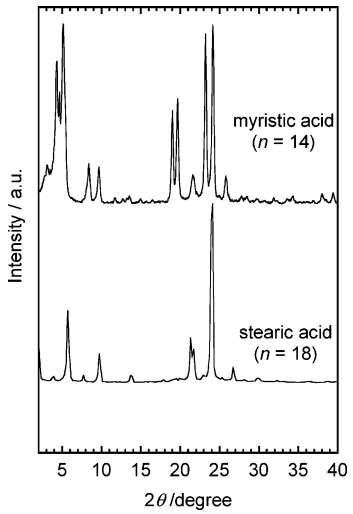

Figure 7. WAXD profiles of myristic acid ($n = 14$) and stearic acid ($n = 18$) measured at 20 °C.

polymer or an entire C_n-AC entity. It is rather plausible to assume that the behavior was caused by some aggregational change restricted to the normal acyl side chains. The magnitude of the thermal signals, irrespective of the endothermic or exothermic inclination of the heat flow, increased with an increase in the side-chain length; this also supports the view that the transition is related only to the side chains.

A feasible interpretation of the pseudo-first-order transitions observed for C_n-ACs of $n \geq 16$ may be an assumption of the usual crystallizing of the normal acyl side chains at comparatively lower temperatures. If this assumption is correct, it follows that the endotherms in the heating scans embodied a crystalline to isotropic phase transition, that is, melting. Then, the crystallizability of the side chains should give rise to some diffraction signals that are essentially similar to those from the corresponding crystalline alkanoic acids at an appropriate temperature range.

In Figure 7, the WAXD profiles of myristic acid ($n = 14$) and stearic acid ($n = 18$) are shown to demonstrate that the fatty acid molecules can crystallize well at room temperature (20 °C) into their distinctive polymorphs.[32−34] On the other hand, Figure 8 displays the WAXD profiles of C_{14}-AC and C_{18}-AC; the data was gathered at different temperatures (−150 to +220 °C) covering the range scanned in the DSC study of transition. Figure 8a indicates that except for an intensity variation of the low-angle diffraction peak, the overall profile of C_{14}-AC solely imparts a diffuse halo centering 18°−20° at any temperature in the measurement range. This observation confirms that the side chains of C_{14}-AC contain no crystalline region, unlike in the case of myristic acid. Similarly, as seen in Figure 8b, none of the WAXD data for C_{18}-AC show any sharp peaks, e.g., at the angular positions of $2\theta = 20°-27°$; this is contrasting to their prominence in the corresponding data for stearic acid per se (Figure 7). These results verify that the side chains of the C_n-ACs ($n \geq 16$) do not cause the crystalline to isotropic phase transition throughout the heating from −150 to +220 °C. Consequently, the transition detected in the DSC thermograms (Figure 6) should be attributed to the emergence of the glass transition as a noncrystallizable material.

Generally, when noncrystalline polymeric materials are annealed at temperatures lower than or comparable to their T_g, the excess amounts of enthalpy and volume decrease with the time required to attain equilibrium so as to render more stable glass materials. This is known as the enthalpy or volume

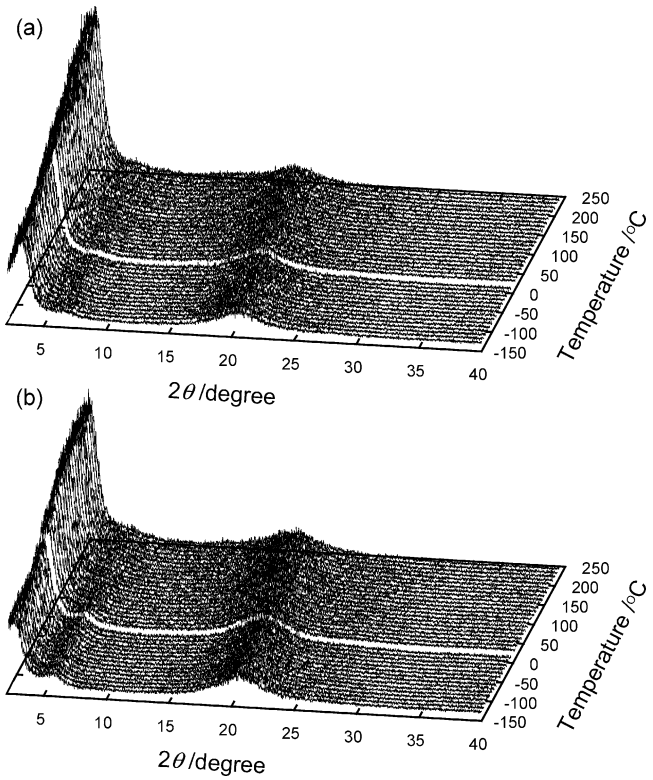

Figure 8. WAXD profiles of (a) C_{14}-AC and (b) C_{18}-AC measured under a thermoregulated condition over a range of −150 to +220 °C.

relaxation of glass-forming polymers[35,36] and commonly termed as the physical aging process. It is thus reasonable to assume that the exotherms and endotherms detected in the DSC cooling and heating cycles for C_n-ACs of $n \geq 16$ represent the enthalpy relaxation and its recovery for the side-chain glasses, respectively. Of particular interest for the present system is the finding that the normal acyl side chains of $n \geq 16$ can reaggregate and relax rapidly to a quasi-equilibrium glassy state without remaining in the state of excess enthalpy for long periods. That is, the enthalpy relaxation occurred during the cooling scan at −20 K min^{-1} and even on quenching (−80 K min^{-1}) to an appreciable extent.

Previously, Sealey and Glasser et al. made similar observations in exotherms and endotherms located between −19 and +55 °C in the DSC measurements for analogous cellulose waxy esters ($n = 14-20$) of DS = 2.8−2.9.[13] They ascribed the transitions to the crystallization and melting of normal acyl side-chain crystals, respectively, with a proviso that it was difficult to accurately ascertain the transition behavior without X-ray diffraction experiments. On the other hand, Zong and Yamane et al. also attributed a similar thermal transition noted for normal acylated chitosans to a semicrystalline structure of the side chains. However, for the present C_n-AC system, no crystalline regularity is induced by the normal acyl side chains, which are confined between chitin trunks layered in intervals of a few nanometers, as has been made evident by the combined use of DSC and thermoregulated WAXD.

Virtually, the supramolecular assemblage of the respective C_n-ACs comprising a chitin trunk polymer and acyl side chains may be regarded as a combination of mesomorphs with nematic and smectic ordering for the trunk and side chains, respectively. In other words, C_n-ACs assume an aggregation structure of "dual mesomorphy". In relation to this depiction, it has been reported that fully acylated celluloses (DS ≈ 3; $n = 8-18$) exhibit a columnar phase, where the cellulosic main chains lie parallel

to the column axis to yield a hexagonal order.[37] The typical phase diagram consists of crystalline solid, mesomorphic, and isotropic regions. On the other hand, the bulk samples of C_n-ACs were continually birefringent at any temperature during heating, eventually undergoing thermal degradation without exhibiting any evident flow. The chitin esters showed poor solubility in common organic solvents such as acetone, tetrahydroflan, dimethyl sulfoxide, DMAc, toluene, and chloroform. These properties of C_n-ACs are in stark contrast to those reported for the cellulosic ester series[13] and aromatic liquid-crystalline polyesters,[25] in which the acylation was conducted to plasticize the respective rigid main-chain polymers. In fact, one of the factors that motivated this study was the expectation of a similar "internal plasticization" of rigid chitinous polymers by longer alkyl substituents. However, why cannot the C3/C6-diesterification of chitin lead to plasticization? We do not have a satisfactory answer to this question. However, it is possible that the almost complete diesterification could cause a suitable conformational symmetry around the chitin backbone axis as well as the growth in the lateral dimension, thereby resulting in the nematic alignment of the main chains as rather stiffer trunks through interlocking between their side chains.

With regard to the thermoregulated WAXD study for C_n-ACs of $n \geq 16$ (see Figure 8), another significant observation is noteworthy: the diffractive peak at the lowest angle ($2\theta < 5°$) gradually became sharper and more intense with increasing temperature, although the 2θ position remained essentially unchanged. This indicates an enhancement in the uniformity of the layered structure of chitinous main-chains at higher temperatures, where the flexibility and, therefore, the thermotropicity of the C_n-ACs appear to be enriched to some extent, despite the flowability, which was still poor as a bulk.

3.4. Kinetics of the Physical Aging of Side Chains. An attempt was made to analyze the strikingly rapid physical aging observed for C_n-ACs of $n = 16-20$ in a more quantitative manner. In general, to evaluate the kinetics of enthalpy relaxation for glassy materials, they are annealed for different aging times under isothermal conditions; therefore, on reheating, the enthalpy recovery is detected as an endothermic peak in the DSC scan. However, the above C_n-AC samples exhibited rapid aging behavior such that the time-course of the relaxation enthalpy could not be traced by the isothermal experiments. Instead, in the present case, the so-called constant cooling rate experiment[38] was conveniently adopted to examine the influence of time scales on the aging of respective samples. As a common practice, this study assumed that the relaxation time τ for enthalpy relaxation of the considered glass depends on both the aging temperature T and a structure-freezing temperature T_f as a fictive factor; this dependence is expressed as follows:[38-41]

$$\tau = \tau_0 \exp\left[\frac{x\Delta h^*}{RT} + \frac{(1-x)\Delta h^*}{RT_f}\right] \tag{3}$$

where τ_0 is the value of τ in equilibrium at infinitely high temperatures; Δh^*, an apparent activation energy for the enthalpy relaxation process; R, the gas constant, and x ($0 \leq x \leq 1$), a nonlinearity parameter[42] reflecting the relative contributions of the external temperature (T) and the internal structure factor (T_f) to the relaxation time.

For the evaluation of the activation energy Δh^*, it is necessary to conduct another DSC experiment, where the sample is cooled at different constant rates before the respective reheating scans at a constant rate. On the other hand, the dependence of the fictive temperature T_f or the glass transition temperature T_g (these are identical if the sample is unaged) on the cooling rate q_1 can be written as follows:[41,42]

$$\frac{d(\ln|q_1|)}{d(1/T_f)} = \frac{-\Delta h^*}{R} \tag{4}$$

The temperature T_f for a given cooling rate is obtained by applying a so-called "equal area" method[41] to an enthalpy recovery signal appearing in the reheating DSC scan. Therefore, the apparent activation energy Δh^* can be determined from the slope of a plot of ln $|q_1|$ versus T_f^{-1}.

According to Angell,[43] glassy materials as well as viscous liquids can be classified for convenience into two categories: strong glasses and fragile ones. It is also pointed out that the strong liquids and glasses form a type of network architecture with developing chemical bonds or interactions as junctions or entanglements, which is usually less sensitive to temperature variation. In contrast, the fragile liquids and glasses are solely made up via van der Waals force and their local structure is significantly affected by temperature variation. The fragility index m of glassy materials is generally defined as in eq 5; a larger m denotes higher fragility.

$$m = \left.\frac{d\log_{10}(\tau)}{d(T_g/T)}\right|_{T=T_g} \tag{5}$$

By using eqs 3 and 5, the fragility index m can be written as

$$m = \frac{\Delta h^*}{RT_g \ln 10} \tag{6}$$

In conventional DSC measurements, T_g of a glassy material is evaluated from the onset (or midpoint) of a baseline shift appearing in a thermogram due to the discontinuity in specific heat that is caused by the material transition on heating. However, this evaluation is severely affected by kinetic effects. To minimize the contribution of such factors, we adopted a method proposed by Richardson et al.[44,45] For this purpose, the ordinary DSC output data of heat flow, shown in Figure 6a, was converted into the corresponding relative enthalpy H, and a plot of H versus temperature was constructed. Subsequently, two tangential lines were drawn on both sides of the glass transition region in the H versus temperature curve, and the temperature value observed at the point of intersection was denoted as T_g. As a result of the regression analysis, the universal T_gs of unaged C_n-ACs of $n = 16$, 18, and 20 were estimated as 230, 244, and 262 K, respectively.

Figure 9 shows the reheating DSC scans for the three C_n-ACs, which were cooled at the indicated rates before the respective scans. Although the thermograms obtained for the same C_n-AC sample resemble each other in shape of the enthalpy recovery peak, a careful analysis by the equal-area method[41] yielded distinctly different T_f values, which shifted systematically with the variation in the pre-cooling rate (q_1). The result is shown in Figure 10 as a plot of ln $|q_1|$ versus T_f^{-1}. A reasonably straight line was drawn to fit the respective plot, which yields Δh^* from the slope (see eq 4). The Δh^* values thus estimated are listed in Table 2 together with the corresponding data assessed for comblike poly(α-*n*-alkyl)acrylates[46] and conventional polymers[46-49] in similar constant cooling rate experiments. The table also contains the respective fragility data calculated by eq 6. Obviously, Δh^*s for the acyl side-chain glasses of the C_n-ACs are much smaller, by 2 or 3 orders of magnitude, as compared with those for the other polymer

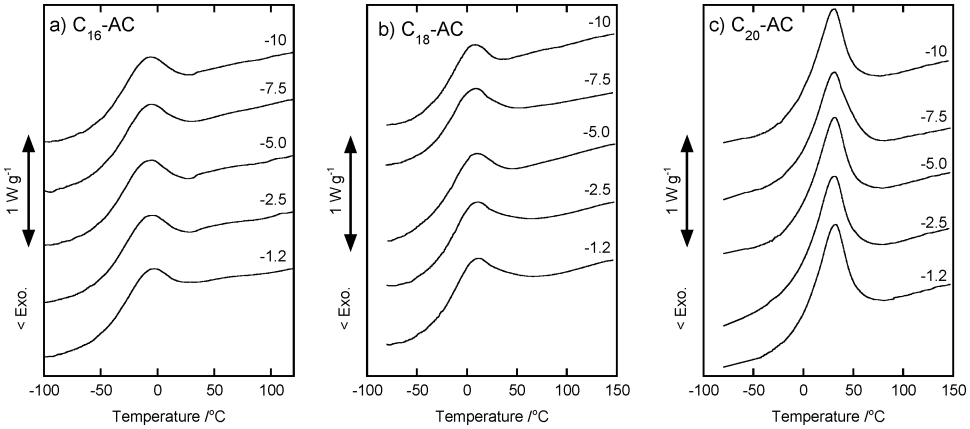

Figure 9. DSC reheating scans at 10 K min^{-1} for three C_n-AC samples, which were conducted immediately after cooling at the indicated rates (in K min^{-1}) from 150 °C to a prescribed temperature of ≤−100 °C.

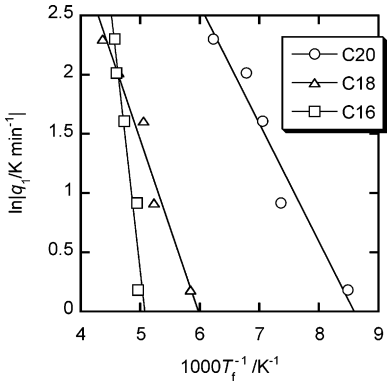

Figure 10. Plots of ln $|q_1|$ vs T_f^{-1} constructed by the analysis of the heating curves shown in Figure 9. Full lines represent the least-squares fitting to the respective data.

Table 2. Activation Energy Δh^* and Fragility Parameter m for C_n-ACs and Glass-Forming Vinyl Polymers Determined by Constant Cooling Rate Experiments

sample	Δh^*/kJ mol^{-1}	T_g/K	m[a]
C_n-ACs			
C_{16}-AC	37	230	8.5
C_{18}-AC	12	244	2.6
C_{20}-AC	8.2	262	1.6
poly(α-*n*-alkyl)acrylate			
C_3[46]	856 ± 74	228[50]	196 ± 17
C_5[46]	524 ± 67	216[50]	126 ± 16
C_8[46]	391 ± 74	208[50]	98 ± 19
poly(methyl methacrylate)[46]	873 ± 74	375	122 ± 10
poly(vinyl acetate)[47]	590	310	99
polystyrene[48]	665	373	93
poly(vinyl chloride)[49]	1122 ± 116	353	166 ± 17

[a] Estimated by eq 6.

glasses. Correspondingly, the m values for the former are also quite low, thereby reflecting the formation of strong glasses. Comparing the three C_n-ACs, we find an appreciable decrease in Δh^* with an increase in the carbon number of the normal acyl side chains.

For further comparison, Table 3 tabulates the result of our previous study on the enthalpy relaxation observed for liquid-crystalline glasses of cholesterol hydrogen phthalate (CHP) and its 1:1 complex salts with normal aliphatic amines (C_n-amines).[51] The phase behavior of these cholesteryl derivatives was quite unique; in particular, it was established that the ionic complexes (CHP/C_n-amine's) with a relatively longer alkyl tail (usually $n > 10$) assumed a glassy state below 30 °C with a frozen smectic-type anisotropic organization, whereas CHP per se (behaving as a dimer unit) formed a cholesteric liquid-crystalline glass. The kinetics of their enthalpy relaxation on aging, slower than that in the case of C_n-ACs, was examined by monitoring the time evolution of the relaxed enthalpy (ΔH) in isothermal DSC experiments. The data analysis was made in terms of a Kohlrausch−Williams−Watts type equation[52] to evaluate the relaxation time τ. Then, the activation energy (E_a) for the isothermal relaxation process was determined from the temperature dependence of τ by using the Arrhenius approximation [$\tau^{-1} = \tau_0^{-1} \exp(-E_a/RT)$]. As can be seen from Table 3, the cholesterol-based mesomorphic glasses also yield considerably lower values of activation energy and fragility as compared with those for amorphous polymer materials. The lowering tendency of E_a and m becomes conspicuous with the increasing carbon number of the C_n-amine component acting as a spacer for the mesogenic steroid core. However, even the E_a value for CHP/C_{18}-amine is still higher than the corresponding values (Δh^*s) for the chitin acylates of $n = 16-20$.

Table 3. Enthalpy Relaxation Data for the Liquid-Crystalline Glasses of CHP and CHP/C_n-Amine Complex Salts Estimated by Isothermal Aging Experiments[a]

glassy sample	E_a/kJ mol^{-1}	T_g/K	m
CHP	154	299	27
CHP/C_{12}-amine	58	284	11
CHP/C_{16}-amine	52	292	9
CHP/C_{18}-amine	47	293	8

[a] Data are all quoted from ref 51.

It is not completely adequate to compare the result for C_n-ACs summarized in Table 2 with that for CHP/C_n-amines because of the difference in thermal treatment. Nevertheless, it may be reasonable to assume that the distinct dual-mesomorphic assemblage of C_n-ACs would cause more rapid and easier relaxation of the acyl side-chain glasses. In other words, the anchoring of the smectic-ordered side chains onto the oriented chitin sustainer should be advantageous for rapidly equilibrating them to a stable glass structure. Deservedly, the spatial restriction can also be a factor of the facilitation. As was demonstrated by WAXD, the normal acyl side chains are confined in the space of a few nanometers by the layered trunk polymers as partitions. Several studies on the dynamics of glass-forming liquids have shown that a spatial confinement in a scale of <10 nm strongly affects the cooperative motions of the constituent molecules.[53−55] In the C_n-AC series ($n \geq 16$) as well, a nanoscopic restraint would occur in the cooperative motions of the side chains, which contributes greatly to the rapid relaxation phenomenon. Thus,

the present system may be an interesting example from the viewpoint of pursuing the nature of glass transition of organic substances.

Finally, annotations should be provided to the thermal behavior of the other C_n-AC samples ($n \leq 14$). The derivatives of $n = 12$ and 14 exhibited a T_g signal associated with their side chains; however, both still did not show such a rapid enthalpy relaxation in the usual DSC scans (see Figure 6). One of the reasons for this is that the vitrification of the side-chain aggregates on cooling occurs under extremely cryogenic conditions, which would be essentially disadvantageous to the progress of glass aging followed by enthalpy relaxation. As another delaying factor, an insufficient spatial allowance would anyway occur for the side chains due to the somewhat shorter length leading to lesser intermolecular digitation. To clarify the side-chain behavior of the two samples, further examination of the physical aging will be required; this would require that an adequate experimental procedure be set up. With regard to the C_n-ACs of $n \leq 10$, there exists a possibility that the glass transition of their side chains may be latent in a region below the temperature limit measurable by the standard DSC analysis. However, considering the stronger anchoring effect and the low overlapping end-to-end packing, it is more plausible that the rather shorter side chains hardly form the glass structure as condensed matter independent of the backbones.

4. Conclusions

In this study, the synthesis of a new series of C_n-ACs was conducted successfully with pyridine, TsCl, and normal alkanoic acids of C_4-C_{20} in a DMAc/LiCl homogeneous system. ^{1}H NMR spectra indicated that the acylation of chitin (p-chitin) occurred preferentially at the O3H or O6H positions of the pyranose ring. Therefore, it can be concluded that nearly saturated diesterification of chitin was attained by this acylation reaction. The WAXD profiles of the acylates at ambient temperature indicated a structural formation in which the chitin trunk polymers were arranged in a layered fashion without showing regularity along their longitudinal axis. Through DSC measurements, the thermal property of the C_n-AC series was characterized by grouping the transitional feature into three classes based on the n value: no evident transition for $n = 4-10$; glass transition centering in a temperature range of -70 to -40 °C for $n = 12$ and 14; and pseudo-first-order phase transition located in a range of -10 to $+30$ °C for $n = 16-20$. It was found that the thermal events actually did not originate from the transitions associated with the trunk part of the chitin acylates, and neither did from their side-chain crystallinity, since there was no substantial dependence of the WAXD profiles of C_n-ACs on temperature in the range of -150 to $+220$ °C, except for the change in peak intensity. Thus, it was reasonably considered that the exotherms and endotherms detected in the cooling and heating DSC scans for $n \geq 16$ represent the enthalpy relaxation and its recovery associated with the side-chain glasses, respectively.

The supramolecular assemblage of C_n-ACs can be virtually regarded as dual mesomorphic; viz., the chitin trunks are solidified in a nematic arrangement and the normal acyl side chains are packed with a smectic order between the trunk layers. By using a conventional analysis of enthalpy relaxation for the longer side chains ($n \geq 16$), it was suggested that the liquid-crystalline glasses would be readily equilibrated with an extremely low activation energy, thereby reflecting an effect of the anchoring and nanospatial confinement of the side chains. However, this holds for the case where the smectic aggregates occupy an adequate space containing a region of intermolecular digitation to a considerable extent. With a decrease in the side-chain length, it becomes difficult for the side chains to form the glass structure as condensed matter separately from the layered backbones, because of the stronger anchoring effect and the less overlapping end-to-end packing. Thus, this may be applicable to the C_n-ACs of $n \leq 10$. In the intermediate case with $n = 12$ and 14, the side chains assumed a glassy state under cryogenic conditions, but hardly exhibited an enthalpy relaxation behavior in the usual DSC scans. The unclear relaxation characteristics leave room for further investigation.

Acknowledgment. The authors acknowledge Dr. Y. Takatsuru of RIGAKU Co. for having afforded the thermoregulated WAXD measurement facilities.

References and Notes

(1) Majeti, N. V.; Kumar, R. *React. Funct. Polym.* **2000**, *46*, 1.
(2) Kurita, K. *Prog. Polym. Sci.* **2001**, *26*, 1921.
(3) Miyashita, Y.; Sato, M.; Kimura, N.; Nishio, Y.; Suzuki, H. *Kobunshi Ronbunshu* **1996**, *53*, 149.
(4) Miyashita, Y.; Kobayashi, R.; Kimura, N.; Suzuki, H.; Nishio, Y. *Carbohydr. Polym.* **1997**, *34*, 221.
(5) Miyashita, Y.; Yamada, Y.; Kimura, N.; Suzuki, H.; Iwata, M.; Nishio, Y. *Polymer* **1997**, *38*, 6181.
(6) Kimura, N.; Sato, M.; Miyashita, Y.; Suzuki, H.; Nishio, Y. *Sen'i Gakkaishi* **1997**, *53*, 409.
(7) Dawsey, T. R. In *Polymer Fiber Science: Recent Advances*; Fornes, R. E., Glbert, R. D., Eds.; VCH: New York, 1992; p 157.
(8) McCormick, C. L.; Lichatowich, D. K. *J. Polym. Sci., Polym. Lett. Ed.* **1979**, *17*, 479.
(9) Terbojevich, M.; Carraro, C.; Cosani, A. *Carbohydr. Res.* **1988**, *180*, 73.
(10) Shigemasa, Y.; Usui, H.; Morimoto, M.; Saimoto, H.; Okamoto, Y.; Minami, S.; Sashiwa, H. *Carbohydr. Polym.* **1999**, *39*, 237.
(11) Kim, J. Y.; Ha, C. S.; Jo, N. J. *Polym. Int.* **2002**, *51*, 1123.
(12) Shimizu, Y.; Hayashi, J. *Cellul. Chem. Technol.* **1989**, *23*, 661.
(13) Sealey, J. E.; Samaranayake, G.; Todd, J. G.; Glasser, W. G. *J. Polym. Sci., Part B: Polym. Phys.* **1996**, *34*, 1613.
(14) Sagar, A. D.; Merrill, E. W. *J. Appl. Polym. Sci.* **1995**, *58*, 1647.
(15) Zong, Z.; Kimura, Y.; Takahashi, M.; Yamane, H. *Polymer* **2000**, *41*, 899.
(16) Hackman, R. H. *Austral. J. Biol. Sci.* **1954**, *7*, 168.
(17) Sannan, T.; Kurita, K.; Ogura, K.; Iwakura, Y. *Polymer* **1978**, *19*, 458.
(18) Nishio, Y.; Roy, S. K.; Manley, R. J. *Polymer* **1987**, *28*, 1385.
(19) Nishio, Y.; Manley, R. J. *Macromolecules* **1988**, *21*, 1270.
(20) Pearson, F. G.; Marchessault, R. H.; Liang, C. Y. *J. Polym. Sci.* **1960**, *43*, 101.
(21) Focher, B.; Naggi, A.; Torri, G.; Cosani, A.; Terbojevich, M. *Carbohydr. Polym.* **1992**, *17*, 97.
(22) Detchprohm, S.; Aoi, K.; Okada, M. *Macromol. Chem. Phys.* **2001**, *202*, 3560.
(23) Jordan, E. F.; Feldeisen, D. W.; Wrigley, A. N. *J. Polym. Sci. A-1* **1971**, *9*, 1835.
(24) Jordan, E. F. *J. Polym. Sci., Part A: Polym. Chem.* **1972**, *10*, 3347.
(25) Platé, N. A.; Shibaev, V. P.; Petrukhin, B. S.; Zubov, Y. A.; Kargin, V. A. *J. Polym. Sci. A-1* **1971**, *9*, 2291.
(26) Morawetz, J.; Catala, J. M.; Lenz, R. W. *Eur. Polym. J.* **1983**, *19*, 1043.
(27) Rodriguez-Parada, J. M.; Duran, R.; Wegner, G. *Macromolecules* **1989**, *22*, 2507.
(28) Lee, J. L.; Pearce, E. M.; Kwei, T. K. *Macromolecules* **1997**, *30*, 6877.
(29) Lee, J. L.; Pearce, E. M.; Kwei, T. K. *Macromolecules* **1997**, *30*, 8233.
(30) Muzzarelli, R. A. A. *Chitin*; Pergamon Press: Oxford, 1977; pp 45–51.
(31) Teramoto, Y.; Nishio, Y. *Biomacromolecules* **2004**, *5*, 397.
(32) Larsson, K.; Sydow, E. *Acta Chem. Scand.* **1966**, *20*, 1203.

(33) Malta, V.; Celotti, G.; Zannetti, R.; Martelli, A. F. *J. Chem. Soc. B* **1971**, 548.
(34) Goto, M.; Asada, E. *Bull. Chem. Soc. Jpn.* **1978**, *51*, 2456.
(35) Weitz, A.; Wunderlich, B. *J. Polym. Sci. Polym. Phys. Ed.* **1974**, *12*, 2473.
(36) Cowie, J. M. G.; Ferguson, R. *Macromolecules* **1989**, *22*, 2307.
(37) Fukuda, T.; Takada, A.; Miyamoto, T. In *Cellulosic Polymers, Blends and Composites*; Gilbert, R. D., Ed.; Hanser Gardner Publications: Munich, 1994; Chapter 3.
(38) Moynihan, C. T.; Easteal, A. J.; DeBolt, M. A.; Tucker, J. J. *J. Am. Ceram. Soc.* **1976**, *59*, 12.
(39) Hodge, I. M. *J. Non-Cryst. Solids* **1994**, *169*, 211.
(40) Tool, A. Q. *J. Am. Ceram. Soc.* **1946**, *29*, 240.
(41) Narayanaswamy, O. S. *J. Am. Ceram. Soc.* **1971**, *54*, 491.
(42) Kovacs, A. J.; Aklonis, J. J.; Hutchinson, J. M.; Ramos, A. R. *J. Polym. Sci., Polym. Phys. Ed.* **1979**, *17*, 1097.
(43) Angell, C. A. *J. Non-Cryst. Solids* **1991**, *131*−*133*, 13.
(44) Kimura, N.; Aizawa, K.; Nishio, Y.; Suzuki, H. *Kobunshi Ronbunshu* **1996**, *53*, 874.
(45) Richardson, M. J.; Savill, N. G. *Polymer* **1975**, *16*, 753.
(46) Godard, M. E.; Saiter, J. M.; Cortés, P.; Montserrat, S.; Hutchinson, J. M.; Burel, F.; Bunel, C. *J. Polym. Sci., Part B: Polym. Phys.* **1998**, *36*, 583.
(47) Sasabe, H.; Moynihan, C. T. *J. Polym. Sci.* **1978**, *16*, 1447.
(48) Hodge, I. M. *Macromolecules* **1987**, *20*, 2897.
(49) Pappin, A. J.; Hutchinson, J. M.; Ingram, M. D. *Macromolecules* **1992**, *25*, 1084.
(50) Brandrup, J., Immergut, E. H., Grulke, E. A., Eds.; *Polymer Handbook*, 4th ed.; John Wiley & Sons: New York, 1999.
(51) Yoshio, M.; Miyashita, Y.; Nishio, Y. *Mol. Cryst. Liq. Cryst.* **2001**, *357*, 27.
(52) Williams, G.; Watts, D. C. *Trans. Faraday Soc.* **1970**, *66*, 80.
(53) Arndt, M.; Stannarius, R.; Groothues, H.; Hempel, E.; Kremer, F. *Phys. Rev. Lett.* **1997**, *79*, 2077.
(54) Huwe, A.; Kremer, F.; Behrens, P.; Schwieger, W. *Phys. Rev. Lett.* **1999**, *82*, 2338.
(55) Adam, G.; Gibbs, J. H. *J. Chem. Phys.* **1965**, *43*, 139.

BM050580Y